

are either weak or non-existent? Long dark spirals like these are unprecedented even for flocculent galaxies. Two possible reasons come to mind. One is related to the extremely large rate of shear in this galaxy, from differential rotation. At the position of the spirals, the rotation speed¹⁷ is a constant $V = 270 \text{ km s}^{-1}$, which is abnormally high for spiral galaxies like ours, and the deprojected radius is $R \approx 5 \text{ kpc}$, which is small compared to the galactocentric radius of the Sun (8.5 kpc) in the Milky Way. The corresponding rate of shear, $Rd(V/R)/dR$, is an enormous $54 \text{ km s}^{-1} \text{ kpc}^{-1}$. This is two times higher than the shear rate in the star-forming parts of the nearby Andromeda galaxy²², its neighbour M33 (ref. 23), and in the solar neighbourhood of our Galaxy. Thus all of the gas features in NGC2841 should be much more spiral-like at the same evolutionary stage than they are in any of these nearby galaxies. We therefore propose that at least some of the dark spirals are simply sheared dark clouds. For a sheared region, the time elapsed from an initially circular state is $R/(V \tan i) = 1.1 \times 10^8 \text{ yr}$ for the observed pitch angle of $i = 9^\circ$ (measured from deprojected images). The mass of each dark spiral is $\sim 10^8 M_\odot$, from the density found in the radiative transfer solution. The dark spirals in NGC2841 are therefore similar in mass to the four largest dust clouds in the Andromeda galaxy²⁴. There are many smaller dark features in NGC2841 as well, which are presumably from smaller sheared clouds.

Another possibility is that some of the dark spirals are weak waves driven in the dusty interstellar medium by non-axisymmetric forces from an elongated bulge. Figure 1b indicates that the bulge in NGC2841 is not aligned along the major axis of the disk—the position angle differs by $\sim 10^\circ$. This means that the bulge is prolate if the disk is circular. Usually prolate bulges appear in barred²⁵ or grand-design galaxies such as Andromeda^{26,27} and NGC4845^{28,29}, where they can excite stellar waves²⁶, but here the stellar disk is apparently too stable for such excitation and the only response is in the dust and gas.

The distinction between sheared clouds and bulge-driven waves

should be evident from velocity measurements of the dark spiral gas. Systematic radial motions outwards or inwards on the minor axis would favour the wave interpretation. □

Received 27 November 1995; accepted 30 April 1996.

1. Elmegreen, D. M. & Elmegreen, B. G. *Astrophys. J. Suppl. Ser.* **54**, 127–150 (1984).
2. Sandage, A. *Hubble Atlas of Galaxies* (Carnegie Instn, Washington DC, 1961).
3. Elmegreen, D. M. & Elmegreen, B. G. *Mon. Not. R. astr. Soc.* **201**, 1021–1034 (1982).
4. Elmegreen, D. M. & Elmegreen, B. G. *Astrophys. J.* **364**, 412–414 (1990).
5. Bertin, G. in *Dynamics of Galaxies and Molecular Cloud Distributions* (eds Combes, F. & Casoli, F.) 93–104 (Kluwer Academic, Dordrecht, 1991).
6. Elmegreen, B. G. & Thomasson, M. *Astr. Astrophys.* **272**, 37–58 (1993).
7. Mark, J. W. K. *Astrophys. J.* **205**, 363–378 (1976).
8. Toomre, A. in *The Structure and Evolution of Normal Galaxies* (eds Fall, S. M. & Lynden-Bell, D.) 111–136 (Cambridge Univ. Press, 1981).
9. Seiden, P. E. & Gerola, H. *Astrophys. J.* **233**, 56–66 (1979).
10. Elmegreen, B. G. & Efremov, Yu. *Astrophys. J.* (in the press).
11. Wainscoat, R. J. & Cowie, L. L. *Astr. J.* **103**, 332–337 (1992).
12. Block, D. L. & Wainscoat, R. J. *Nature* **353**, 48–50 (1991).
13. Block, D. L. *et al.* *Astrophys.* **288**, 365–382 (1994).
14. Rix, H.-W. & Zaritsky, D. *Astrophys. J.* **418**, 123–134 (1993).
15. Rix, H.-W. & Zaritsky, D. in *Infrared Astronomy with Arrays: The Next Generation* (ed. McLean, I. S.) 151–152 (Kluwer Academic, Dordrecht, 1994).
16. Wray, J. D. *The Color Atlas of Galaxies* (Cambridge Univ. Press, 1988).
17. Bosma, A. *Astr. J.* **86**, 1825–1846 (1981).
18. Begeman, K. G. thesis, Univ. Groningen (1987).
19. Young, J. S. & Scoville, N. *Astrophys. J.* **260**, L41–L44 (1982).
20. Braine, J. & Combes, F. *Astr. Astrophys.* **264**, 433–443 (1992).
21. Block, D. L., Witt, A. N. & Grosbøl, P. in *The Opacity of Spiral Disks* (eds Davies, J. I. & Burstein, D.) 227–242 (Kluwer Academic, Dordrecht, 1995).
22. Brinks, E. & Burton, W. B. *Astr. Astrophys.* **141**, 195–214 (1984).
23. Deul, E. R. & van der Hulst, J. M. *Astr. Astrophys. Suppl. Ser.* **67**, 509–539 (1987).
24. Hodge, P. W. *Astr. J.* **85**, 376–386 (1980).
25. Wozniak, H., Friedli, D., Martinet, L., Martin, P. & Bratschi, P. *Astr. Astrophys. Suppl. Ser.* **111**, 115–152 (1995).
26. Stark, A. A. *Astrophys. J.* **213**, 368–373 (1977).
27. Lindblad, B. *Stockholm Obs. Ann.* **19**(2), 1–12 (1956).
28. Bertola, F., Rubin, V. C. & Zeilinger, W. W. *Astrophys. J.* **345**, L29–L32 (1989).
29. Gerhard, O. E., Vietri, M. & Kent, S. M. *Astrophys. J.* **345**, L33–L36 (1989).
30. Witt, A. N., Lindell, R. S., Block, D. L. & Evans, Rh. *Astrophys. J.* **427**, 227–231 (1994).

ACKNOWLEDGEMENTS. Figure 1a is reproduced by permission of the Carnegie Institution of Washington and the California Institute of Technology. Figure 1b was made using the IBM Image Access Executive. Figure 1c was made using Data Explorer with the help of C. Pickover. The V image used for Fig. 2 was kindly supplied by A. Heller and N. Brosch. We thank S. Courteau, D. Elmegreen, and S. Federman for discussions, and F. Combes and K. G. Begeman for supplying gas column densities in tabular form.

Giant oxygen isotope shift in the magnetoresistive perovskite $\text{La}_{1-x}\text{Ca}_x\text{MnO}_{3+y}$

Guo-meng Zhao*, K. Conder†, H. Keller* & K. A. Müller*

* Physik-Institut der Universität Zürich, CH-8057 Zürich, Switzerland
† Laboratorium für Festkörperphysik ETH Zürich, CH-8093, Switzerland

FERROMAGNETIC perovskites of the form $\text{La}_{1-x}\text{Me}_x\text{MnO}_{3-y}$ (where Me is Ca or Sr) have been known¹ since 1950, but there has been a recent resurgence of interest following the discovery of giant magnetoresistance in this class of compounds^{2,3}. The compounds contain both Mn^{3+} and Mn^{4+} ions; as the electronic ground state of the Mn^{3+} ions is degenerate, their energy is lowered by a spontaneous distortion of the surrounding lattice—the Jahn–Teller effect⁴. The charge carriers in these materials are strongly coupled to (and mediate the ferromagnetic interaction between) the manganese ions⁵, suggesting that localized lattice distortions could also play an important role in determining the electronic and magnetic properties of these compounds. Here we investigate this possibility by examining the effect on the ferromagnetic transition temperature of varying the oxygen isotope mass (replacing ^{16}O with ^{18}O). For $\text{La}_{0.8}\text{Ca}_{0.2}\text{MnO}_{3+y}$, we measure an isotope shift of $>20 \text{ K}$, significantly larger than that found for any magnetic or electronic phase transition in other oxides. In contrast, we observe no significant isotope shift for the structurally related ferromagnet SrRuO_3 , in which the Jahn–Teller

effect is negligible. These results imply that the large isotope shift arises from coupling of the charge carriers to Jahn–Teller lattice distortions, and we suggest that such Jahn–Teller ‘polarons’ may also be responsible for the magnetoresistive properties of these materials.

In 1983, Höck *et al.*⁶ studied Jahn–Teller (JT) ions in a conductor within a linear chain model. They showed that a small JT polaron (the combination of the electron and induced lattice distortion around it) can be formed when the JT stabilization energy is comparable with the bare conduction bandwidth. This is due to the breakdown of the Born–Oppenheimer adiabatic approximation in which the electronic and lattice subsystems are decoupled. The JT polaron is induced by the electronic ground-state degeneracy rather than by a charge polarization that may induce a dielectric polaron.

The polaronic nature of the conduction carriers can be demonstrated by the isotope effect on the effective bandwidth W_{eff} of polarons, which in turn depends on the isotope mass⁷:

$$W_{\text{eff}} \propto W \exp(-\gamma E_b/\hbar\omega) \quad (1)$$

Here W is the bare conduction bandwidth, E_b is the binding energy of the polaron (independent of the isotope mass), ω is the characteristic frequency of the optical phonons depending on the isotope mass M ($\omega \propto M^{-1/2}$). The dimensionless parameter γ is a function of E_b/W with $0 < \gamma \leq 1$; as E_b/W decreases, γ decreases and W_{eff} increases. For JT polarons, the binding energy of polarons E_b can be replaced by the JT stabilization energy E_{JT} (ref. 8). As the JT state of Mn^{3+} has a sizeable E_{JT} of $\sim 0.5 \text{ eV}$ (ref. 9), one would expect from equation (1) that the isotope effect on W_{eff} is substantial in the manganites.

In the ferromagnetic manganites such as $\text{La}_{1-x}\text{Ca}_x\text{MnO}_{3+y}$, it is

easy to study the isotope effect on W_{eff} . This is due to the fact that in the strong-coupling limit, where the Hund's-rule coupling J_H is very large compared to W_{eff} ($J_H \gg W_{\text{eff}}$), the Curie temperature $T_c \propto W_{\text{eff}}$ (refs 5,9). The isotope dependence of W_{eff} can also be investigated in a ferromagnet as SrRuO_3 , where T_c depends strongly on W_{eff} , as indicated by a large pressure effect¹⁰. In the ferromagnet SrRuO_3 , however, the JT effect is very weak, so the isotope dependence of W_{eff} might be very weak. Therefore, studies of the oxygen isotope effect on the Curie temperature in these ferromagnets can assess the importance of the JT effect in the formation of polarons. This will also give an important insight into the microscopic origin of the colossal magnetoresistance (CMR) effect.

Samples of $\text{La}_{1-x}\text{Ca}_x\text{MnO}_{3+y}$ were prepared by conventional solid-state reaction using La_2O_3 , CaCO_3 and MnO_2 . The powders were mixed, ground thoroughly and heated in air at $1,050^\circ\text{C}$ for ~ 20 h. The samples were then pressed into pellets, and sintered in air at $1,080^\circ\text{C}$ for ~ 48 h. Similar conditions were used for preparing samples of SrRuO_3 . The samples are single-phase, as checked by X-ray diffraction. The ^{16}O and ^{18}O samples were prepared from the same batch of the starting material, and were subjected to the same thermal treatment in closed ampoules (one was filled with $^{16}\text{O}_2$ gas, and another with $^{18}\text{O}_2$ gas)¹¹. The diffusion was carried out for 48 h at 950°C and in an oxygen pressure of ~ 1.0 bar. The difference between the oxygen partial pressures of the ^{16}O and ^{18}O ampoules was less than 4%. The cooling was very slow, with a rate of 30°C h^{-1} . The oxygen-isotope enrichment was determined from the weight changes of both ^{16}O and ^{18}O samples. The ^{18}O samples of $\text{La}_{1-x}\text{Ca}_x\text{MnO}_{3+y}$ had $\sim 95\%$ ^{18}O and $\sim 5\%$ ^{16}O . The ^{18}O samples of SrRuO_3 had $80 \pm 15\%$ ^{18}O and $20 \pm 15\%$ ^{16}O .

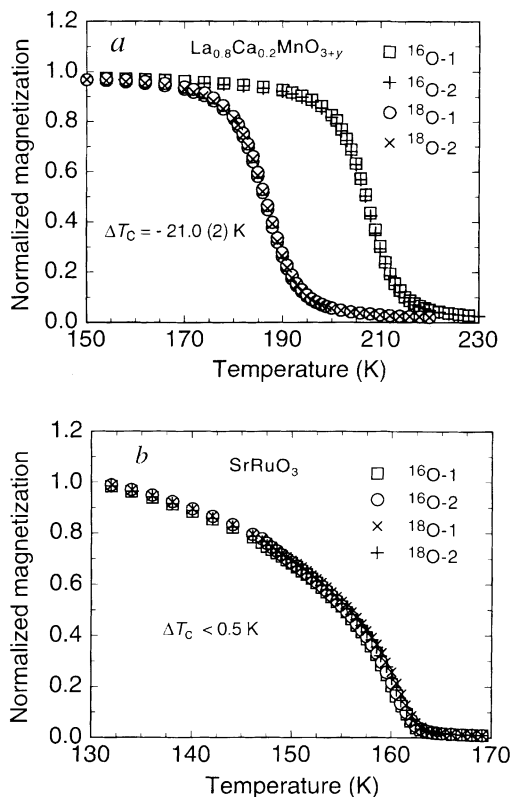


FIG. 1 Oxygen isotope effect on the Curie temperature of $\text{La}_{0.8}\text{Ca}_{0.2}\text{MnO}_{3+y}$ and SrRuO_3 : temperature dependence of the normalized magnetization for ^{16}O and ^{18}O samples of $\text{La}_{0.8}\text{Ca}_{0.2}\text{MnO}_{3+y}$ (a) and SrRuO_3 (b). There is a large oxygen isotope effect on Curie temperature (~ 21 K) in $\text{La}_{0.8}\text{Ca}_{0.2}\text{MnO}_{3+y}$ with a strong JT effect, but no observable effect in the ferromagnet SrRuO_3 with a negligible JT effect. Note that the two independent ^{16}O samples (as well as the two independent ^{18}O samples) have the same T_c , demonstrating an excellent reproducibility of the isotope experiments.

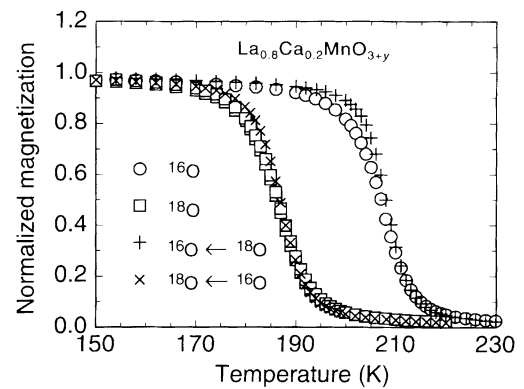


FIG. 2 Oxygen back-exchange result for sample pair ^{16}O -1/ ^{18}O -1 (see Fig. 1a): temperature dependence of the normalized magnetization for ^{16}O and ^{18}O samples of $\text{La}_{0.8}\text{Ca}_{0.2}\text{MnO}_{3+y}$ before and after oxygen back-exchange. The symbol '+' denotes the ^{16}O sample which has been back-exchanged from the original ^{18}O sample (denoted by open square). The symbol 'x' represents the ^{18}O sample which has been back-exchanged from the original ^{16}O sample (denoted by open circle). It is evident that the T_c of the ^{16}O (^{18}O) sample goes back completely to that of the original ^{18}O (^{16}O) sample after the oxygen back-exchange.

The field-cooled magnetization of the samples was measured with a commercial SQUID magnetometer in a field of 5 mT. The samples were cooled directly to 5 K, then warmed to a temperature well below T_c and maintained at that temperature for 20 minutes. Data were collected on warming to a temperature well above T_c . The magnetic field was kept unchanged throughout each series of measurements. In Fig. 1 we show the magnetization (normalized to the magnetization well below T_c) for pairs of ^{16}O and ^{18}O samples (that is, two for each isotope) of $\text{La}_{0.8}\text{Ca}_{0.2}\text{MnO}_{3+y}$ (Fig. 1a) and SrRuO_3 (Fig. 1b). The oxygen isotope shifts of T_c were determined from the differences between the midpoint temperatures on the transition curves of the ^{16}O and ^{18}O samples. For the CMR ferromagnet $\text{La}_{0.8}\text{Ca}_{0.2}\text{MnO}_{3+y}$, the ^{18}O samples have lower T_c s than the ^{16}O samples by ~ 21 K, whereas the two ^{16}O samples (as well as the two ^{18}O samples) have the same T_c . On the other hand, no oxygen isotope effect on T_c could be detected in the ferromagnet SrRuO_3 with a negligible JT effect. If we define the oxygen isotope exponent as $\alpha_o = -\ln T_c / \ln M_o$ (where M_o is the oxygen isotope mass), then we obtain $\alpha_o \approx 0.85$ for $\text{La}_{0.8}\text{Ca}_{0.2}\text{MnO}_{3+y}$. For $\text{La}_{0.9}\text{Ca}_{0.1}\text{MnO}_{3+y}$, we found a slightly smaller exponent $\alpha_o \approx 0.70$ ($T_c \approx 140$ K, $\Delta T_c = 11.7(2)$ K). These exponents are considerably larger than those recently observed in the Sr-doped system $\text{La}_{1-x}\text{Sr}_x\text{MnO}_{3+y}$ (for example, $\alpha_o = 0.19$ for $x = 0.10$; $\alpha_o = 0.14$ for $x = 0.15$; $\alpha_o = 0.07$ for $x = 0.3$; G.M.Z. and D. E. Morris, unpublished results).

To show that the observed oxygen isotope shifts are intrinsic, we have performed oxygen back-exchange experiments ($^{16}\text{O} \rightarrow ^{18}\text{O}$; $^{18}\text{O} \rightarrow ^{16}\text{O}$). In Fig. 2 we show the normalized magnetization for the ^{16}O and ^{18}O samples of $\text{La}_{0.8}\text{Ca}_{0.2}\text{MnO}_{3+y}$ before and after oxygen back-exchange. It is evident that the T_c of the ^{16}O (^{18}O) sample goes back completely to that of the original ^{18}O (^{16}O) sample after the oxygen back-exchange. This clearly indicates that the shift of T_c is caused only by changing the oxygen isotope mass.

It is also important to check whether the observed isotope shifts may arise from a difference in the oxygen contents of the ^{16}O and ^{18}O samples. We think this is very unlikely for the following reasons. First, the T_c of the $\text{La}_{1-x}\text{Ca}_x\text{MnO}_{3+y}$ system is hardly changed even after some extreme thermal treatments (for example, annealing under 200 bar of oxygen pressure at $\sim 600^\circ\text{C}$ and quenching from $1,300^\circ\text{C}$)¹², and the present ^{16}O and ^{18}O samples were treated under the same thermal condition. Second, the ^{16}O and ^{18}O samples of the related $\text{La}_{2-x}\text{Sr}_x\text{CuO}_{4+y}$ compound were shown to have the same oxygen contents by comparing the lattice

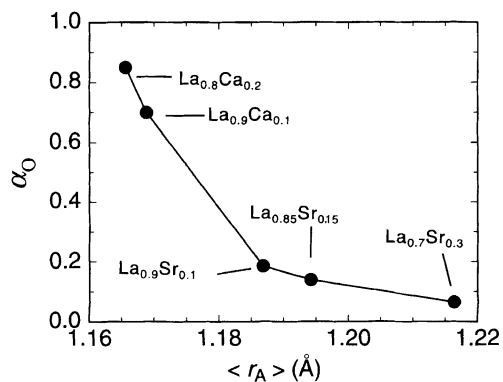


FIG. 3 The dependence of the oxygen isotope exponent α_O on the average ionic radius $\langle r_A \rangle$ at the cation site $\text{La}_{1-x}\text{Me}_x$. (The results for the Sr-doped compounds are unpublished results of G.M.Z. and D. E. Morris.) The solid line is to guide the eye. The isotope exponent α_O increases rapidly with decreasing $\langle r_A \rangle$.

constants of the two isotope samples¹³. For the present CMR materials, we have used the same oxygen-isotope exchange procedure as for the $\text{La}_{2-x}\text{Sr}_x\text{CuO}_{4+y}$ compound, so we expect that the oxygen contents of the present ^{16}O and ^{18}O samples are the same as well.

We now consider why the oxygen isotope exponents α_O in Ca-doped $\text{La}_{1-x}\text{Ca}_x\text{MnO}_{3+y}$ are much larger than those in Sr-doped $\text{La}_{1-x}\text{Sr}_x\text{MnO}_{3+y}$. This may be due to the difference in the ionic radii of Ca^{2+} and Sr^{2+} . In Fig. 3 we show the dependence of α_O on the average ionic radius $\langle r_A \rangle$ at the cation site $\text{La}_{1-x}\text{Me}_x$. The ionic radii of $\text{La}_{1-x}\text{Me}_x$ were calculated from tabulated values (La^{3+} , 1.172 Å; Ca^{2+} , 1.140 Å; Sr^{2+} , 1.320 Å; ref. 14). It is evident that α_O increases rapidly with decreasing $\langle r_A \rangle$. Although α_O may also depend on the Mn^{4+} concentrations, it is clear from Fig. 3 that $\langle r_A \rangle$ has a dominant effect on the value of α_O . A similar correlation between the magnitude of the magnetoresistance and $\langle r_A \rangle$ has recently been reported by Hwang *et al.*¹⁵; they showed that the magnetoresistance decreases rapidly with increasing $\langle r_A \rangle$. Thus, the oxygen-isotope exponent α_O is correlated with the magnitude of magnetoresistance.

As there is no oxygen-isotope effect on T_c in the ferromagnet SrRuO_3 which has a negligible JT effect, the giant isotope effect observed in the Ca-doped ferromagnets is very likely to be related to the strong JT effect in this system. For a compound with a strong JT effect, the electron-phonon interaction is also large, leading to the formation of JT polarons⁶. Taking into account that the binding energy of polarons E_b in the JT compound is equal to the JT stabilization energy E_{JT} (ref. 8), and $T_c \propto W_{\text{eff}}$ for $J_H \gg W_{\text{eff}}$, equation (1) gives

$$T_c \propto W \exp(-\gamma E_{JT}/\hbar\omega) \quad (2)$$

The total isotope exponent is then given by

$$\alpha = -\ln T_c / \ln M = 0.5\gamma E_{JT}/\hbar\omega \quad (3)$$

Because γ increases with increasing E_{JT}/W (ref. 7) equation (3) indicates that the isotope exponent increases with increasing E_{JT} , but decreases with increasing W . For the manganites, an increase in $\langle r_A \rangle$ usually enhances the covalency of the Mn-O bonding¹⁶, and hence increases the bare conduction bandwidth W , leading to a decrease of α . This mechanism naturally explains why the oxygen-isotope exponent α_O increases with decreasing $\langle r_A \rangle$, as shown in Fig. 3.

Our results thus strongly suggest that in the CMR manganites there is a substantial JT effect and thus a large electron-phonon interaction which leads to the formation of JT polarons⁶. This is also consistent with a recent theoretical study of the JT lattice coupling effects in the CMR manganites¹⁷. For the ferromagnet SrRuO_3 with a negligible JT effect, the electron-phonon interaction

may be very small, so that no polarons are formed. That is why no oxygen isotope effect on the Curie temperature is observed in the ferromagnet SrRuO_3 . □

Received 8 March; accepted 9 May 1996.

- Jin, S. *et al. Science* **264**, 413–415 (1994).
- Jonker, G. H. & Van Santen, J. H. *Physica* **16**, 337–349 (1950).
- Chahara, K. *et al. Appl. Phys. Lett.* **63**, 1990–1992 (1993). (see note below)
- Jahn, H. A. & Teller, E. *Proc. R. Soc. Lond. A* **161**, 220–235 (1937).
- Anderson, P. W. & Hasegawa, H. *Phys. Rev.* **100**, 675–681 (1955).
- Höck, K.-H., Nickisch, H. & Thomas, H. *Helv. phys. Acta* **50**, 237–243 (1983).
- Alexandrov, A. S. & Mott, N. F. *Int. J. mod. Phys. B* **8**, 2075–2109 (1994).
- De Jongh, L. J. *Physica C* **152**, 171–216 (1988).
- Millis, A. J., Littlewood, P. B. & Shraiman, B. I. *Phys. Rev. Lett.* **74**, 5144–5147 (1995).
- Shikano, M. *et al. Solid St. Commun.* **90**, 115–119 (1994).
- Zech, D. *et al. Nature* **371**, 681–683 (1994).
- Schiffer, P. *et al. Phys. Rev. Lett.* **75**, 3336–3339 (1995).
- Zhao, G. M. *et al. Phys. Rev.* **B52**, 6840–6844 (1995).
- Shannon, R. D. *Acta crystallogr.* **A32**, 751–767 (1976).
- Hwang, H. Y. *et al. Phys. Rev. Lett.* **75**, 914–917 (1995).
- Goodenough, J. B. *Phys. Rev.* **106**, 564–573 (1955).
- Röder, H., Zhang, J. & Bishop, A. R. *Phys. Rev. Lett.* **76**, 1356–1359 (1996).

ACKNOWLEDGEMENTS. This work was supported by the Swiss National Science Foundation.

Exceptionally high Young's modulus observed for individual carbon nanotubes

M. M. J. Treacy*, T. W. Ebbesen* & J. M. Gibson†

*NEC Research Institute, Inc., 4 Independence Way, Princeton, New Jersey 08540, USA

†University of Illinois, Department of Physics, 1110 West Green Street, Urbana, Illinois 61801, USA

CARBON nanotubes are predicted to have interesting mechanical properties—in particular, high stiffness and axial strength—as a result of their seamless cylindrical graphitic structure^{1–5}. Their mechanical properties have so far eluded direct measurement, however, because of the very small dimensions of nanotubes. Here we estimate the Young's modulus of isolated nanotubes by measuring, in the transmission electron microscope, the amplitude of their intrinsic thermal vibrations. We find that carbon nanotubes have exceptionally high Young's moduli, in the terapascal (TPa) range. Their high stiffness, coupled with their low density, implies that nanotubes might be useful as nanoscale fibres in strong, lightweight composite materials.

Large bundles of carbon nanotubes were teased from a core

TABLE 1 Properties of individual nanotubes

Nanotube no.	Length (μm)	Outer diameter (nm)	Inner diameter (nm)	Young's modulus (TPa)
1	1.17	5.6	2.3	1.06
2	3.11	7.3	2.0	0.91
3	5.81	24.8	6.6	0.59
4	2.65	11.9	2.0	1.06
5	1.73	7.0	2.3	2.58
6	1.53	6.6	2.3	3.11
7	2.04	7.0	3.0	1.91
8	1.43	6.6	3.3	4.15
9	0.66	7.0	3.3	0.42
10	1.32	9.9	3.0	0.40
11	5.10	8.4	1.0	3.70

Average value of Young's modulus is 1.8 TPa.